doi:10.1016/j.jmb.2007.01.039 J. Mol. Biol. (2007) 367, 1186–1204

JMB

Available online at www.sciencedirect.com

ScienceDirect

ELSEVIER

Mechanism of Formation of Amyloid Protofibrils of Barstar from Soluble Oligomers: Evidence for Multiple Steps and Lateral Association Coupled to Conformational Conversion

Santosh Kumar, Subhendu K. Mohanty and Jayant B. Udgaonkar*

National Centre for Biological Sciences, Tata Institute of Fundamental Research, GKVK Campus, Bangalore 560 065 India

Understanding the heterogeneity of the soluble oligomers and protofibrillar structures that form initially during the process of amyloid fibril formation is a critical aspect of elucidating the mechanism of amyloid fibril formation by proteins. The small protein barstar offers itself as a good model protein for understanding this aspect of amyloid fibril formation, because it forms a stable soluble oligomer, the A form, at low pH, which can transform into protofibrils. The mechanism of formation of protofibrils from soluble oligomer has been studied by multiple structural probes, including binding to the fluorescent dye thioflavin T, circular dichroism and dynamic light scattering, and at different temperatures and different protein concentrations. The kinetics of the increase in any probe signal are single exponential, and the rate measured depends on the structural probe used to monitor the reaction. Fastest is the rate of increase in the mean hydrodynamic radius, which grows from a value of 6 nm for the A form to 20 nm for the protofibril. Slower is the rate of increase in thioflavin T binding capacity, and slowest is the rate of increase in circular dichroism at 216 nm, which occurs at about the same rate as that of the increase in light scattering intensity. The dynamic light scattering measurements suggest that the A form transforms completely into larger size aggregates at an early stage during the aggregation process. It appears that structural changes within the aggregates occur at the late stages of assembly into protofibrils. For all probes, and at all temperatures, no initial lag phase in protofibril growth is observed for protein concentrations in the range of 1 μM to 50 μM. The absence of a lag phase in the increase of any probe signal suggests that aggregation of the A form to protofibrils is not nucleation dependent. In addition, the absence of a lag phase in the increase of light scattering intensity, which changes the slowest, suggests that protofibril formation occurs through more than one pathway. The rate of aggregation increases with increasing protein concentration, but saturates at high concentrations. An analysis of the dependence of the apparent rates of protofibril formation, determined by the four structural probes, indicates that the slowest step during protofibil formation is lateral association of linear aggregates. Conformational conversion occurs concurrently with lateral association, and does so in two steps leading to the creation of thioflavin T binding sites and then to an increase in β-sheet structure. Overall, the study indicates that growth during protofibril formation occurs step-wise through progressively larger and larger aggregates, *via*

Abbreviations used: AFM, atomic force microscopy; DLS, dynamic light scattering.

E-mail address of the corresponding author: jayant@ncbs.res.in

multiple pathways, and finally through lateral association of critical aggregates.

Keywords: barstar; amyloid protofibrils; soluble oligomers; lateral association; multiple pathways

*Corresponding author

Introduction

Amyloid fibrils are thread-like stable nanostructures that can be adopted by polypeptide chains.[1] They are formed by the self-assembly of many different peptides and proteins, some of which are involved in human diseases. Structural characterization of amyloid fibrils is not easy, because they are typically insoluble and heterogeneous; nevertheless, there has been significant recent progress. Solid-state NMR has been particularly useful in identifying distinct structures in amyloid fibrils.[2,3] The first structure determined by X-ray crystallography,[4] of an engineered peptide amyloid fibril, has provided a definitive confirmation of the presence of the cross-β motif, in which the core region is formed from β-strands oriented perpendicular and β-sheets oriented parallel to the fibril axis. This motif is thought to be a generic feature of all amyloid fibrils.[5] HX-NMR studies have allowed identification of the structure and the heterogeneity of the amyloid core,[6–8] have suggested that amyloid fibrils could be dynamic structures with protein molecules constantly exchanging between fibril and solution,[9] and have provided three-dimensional structures in conjunction with mutagenesis and solid-state NMR studies.[10,11] Fluorescence methods too have assisted in the determination of amyloid structure.[12,13]

Amyloid fibrils of the same protein may possess structural variations;[2,3] some of them are subtle, which may arise, for example, when fibril formation occurs under different conditions. Fibrils formed from the same protein can differ in the number of protofilaments that comprise the mature fibril[14] as well as in the helicity of their intertwining. It appears that a specific structural variant can confer its own structure on other protein molecules capable of assembly into fibrils, thereby propagating itself as a strain.[3,15–18] Obtaining an insight into the origin of heterogeneity in amyloid structures will follow from an understanding of the mechanism of fibril assembly, and the heterogeneity that is inherent in this process.

Soluble spherical oligomers, as well as either elongated or circularized beaded structures referred to as protofibrils,[19–28] are observed frequently during the assembly of amyloid fibrils, and it is important to define their roles in any model for fibril formation. A crucial question is whether they are productive assembly intermediates[19,25,29] or whether they are merely off-pathway products formed in competition with fibrils.[21,30,31] The lag phase observed commonly in the kinetics of fibril formation appears to be associated with the formation of soluble oligomers and protofibrils from partially structured monomeric intermediates,[19,32,33] but it is possible that these oligomers then dissociate into monomeric species that add to the growing protofibrils or fibrils.

It now appears that it is the soluble oligomer or protofibril, rather than the insoluble fibril, which may be the toxic species in amyloid related human diseases.[34–37] Hence, no matter what exact role the smaller soluble protein aggregates play in the formation of amyloid fibrils, it has become imperative to understand the structural heterogeneity that characterizes the initial assembly of amyloid fibrils, and to understand how the smaller soluble aggregates convert into protofibrils.

The small protein barstar (Figure 1) has been used extensively as a model protein for protein folding and unfolding studies, and it offers much promise as a model protein for studying the mechanism of amyloid formation. It forms a soluble oligomer, the A form, at low pH, which has been characterized extensively. The A form has been shown to be a 16-mer, molten globule-like in possessing partial secondary and a strongly perturbed tertiary structure, as detected by circular dichroism and time-resolved fluorescence studies.[38–40] In the 16-mer, the monomeric units are arranged symmetrically, and the 16

Figure 1. The structure of barstar. Barstar consists of three parallel β-strands and four α-helices. The positions of the three tryptophan residues (38, 44, and 53) are shown. The diagram was generated from PDB file 1btb using Rasmol.

N-terminal segments have full conformational freedom,[41] suggesting the possibility of a reverse micellar structure.[42] The easily studied A form has been shown to transform first into amyloid protofibrils, and then into fibrils, upon heating[13,43] or upon addition of destabilizing agents such as trifluoroethanol (unpublished results). Given the difficulty in studying pre-fibrillar oligomers in the case of other proteins, especially those associated with diseases, the barstar system is attractive from the viewpoint of studying amyloid formation, because of the relative ease with which both formation of the soluble pre-fibrillar oligomers and the conversion of soluble oligomers to protofibrils can be studied. Moreover, the mechanism of protein unfolding has been well-studied, and unfolding intermediates are well characterized.[44–48] This is important, and enhances the attractiveness of using barstar for studying amyloid formation, because it is starting with a partially unfolded monomeric form that a protein begins to aggregate.[49]

Here, the transformation of the A form to protofibrils has been studied using four different probes for structure: thioflavin T (ThT)-binding ability, circular dichroism (CD) at 216 nm, mean apparent hydrodynamic radius, and total light scattering intensity. It is seen that the transformation of the A form into amyloid protofibrils occurs by seemingly simple single exponential kinetics, with no lag phase apparent in the kinetics measured over a wide range of temperature and protein concentration. The process does not appear to be nucleation dependent. Different structural probes yield different apparent rate constants for the transformation of the A form to the protofibrils, indicating that the transformation occurs in steps. An analysis of the kinetics of aggregation by the different probes, and their dependence on protein concentration, indicates that the conversion of the soluble A form oligomer to protofibrils occurs through aggregates of gradually increasing size, and finally through association of critical oligomers. Moreover, it appears that different transient aggregates, which differ in size, define competing pathways for the formation of protofibrils.

Results

The A form is transformed into amyloid protofibrils at low pH

Upon a jump in pH from pH 8 to 2.7, native barstar is transformed into the oligomeric A form. When measured by the accompanying change in the intrinsic Trp fluorescence, the process takes 1 h to complete (data not shown). The size of the A form, as measured by dynamic light scattering, does not change even after an incubation of 12 h at 25 °C (data not shown). In the experiments reported here, the A form is incubated at 25 °C for 6 h at pH 2.7, before the formation of protofibrils is initiated by a temperature jump.

In the absence of added protein, thioflavin T shows maximum fluorescence emission at 430 nm. When barstar is heated to 60 °C at pH 2.7 for 3 h, and added to the dye, the wavelength of maximum fluorescence emission of the dye is seen to shift to 482 nm (Figure 2(a)). Such a shift is characteristic of the binding of thioflavin T with amyloid fibril-like structures. In the assay conditions, the dye concentration was typically in fivefold excess over the protein concentration. When the ratio of dye to protein present in the assay, is reduced, keeping the dye concentration constant, the thioflavin T fluorescence is seen to be proportional to the protein concentration (Figure 2(a), inset). Even at a dye to protein ratio of 5:4, it appears that the amount of dye is sufficient to bind to all the available binding sites. In another study (data not shown), when the protein concentration in the assay solution was kept fixed at 1 μM, and the thioflavin T concentration was varied between 5 μM and 50 μM, the fluorescence emission intensity at 482 nm was found not to change, indicating that a fivefold excess of the dye is sufficient to saturate all the binding sites.

Figure 2(b) shows an atomic force microscopy (AFM) image of barstar that had been heated to 60 °C at pH 2.7 for 3 h. Short curly, worm-like nanostructures are seen, which are commonly referred to as protofibrils.

The data in Figure 2(a) and (b) indicate that upon heating to 60 °C at pH 2.7 for 3 h, the A form is converted to protofibrils.

Figure 2(c) shows the kinetics of formation of amyloid protofibrils at 60 °C, monitored by measurement of the increase in thioflavin T fluorescence (at 482 nm) upon binding. The kinetics show that there is no observable lag phase, and can be described well as single exponential. The inset to Figure 2(c) shows that the formation of protofibrils also occurs at 25 °C, albeit to a much lesser extent, and much more slowly. The inset also shows that the kinetics of protofibril formation at 25 °C are identical at pH 2.7 and pH2, and that no detectable transformation of the native protein into protofibrils occurs at pH 8 even upon a prolonged incubation. At pH 8, there is no detectable conversion of the native protein into protofibrils, even at higher temperatures (data not shown).

Figure 2(d) shows the kinetics of formation of amyloid protofibrils, determined by measurement of the change in ellipticity at 216 nm. Again, no initial lag is observed in the kinetics, and the kinetics are well described as single exponential. A comparison of Figure 2(c) and (d) indicates that the ellipticity-monitored kinetics are significantly slower than the thioflavin T fluorescence-monitored kinetics.

In Figure 2(c) and (d), the extent of aggregation at each time point is reported as the mean of three separate measurements. The relatively small standard deviation observed indicates that the extent of aggregation measured at any time using either of the

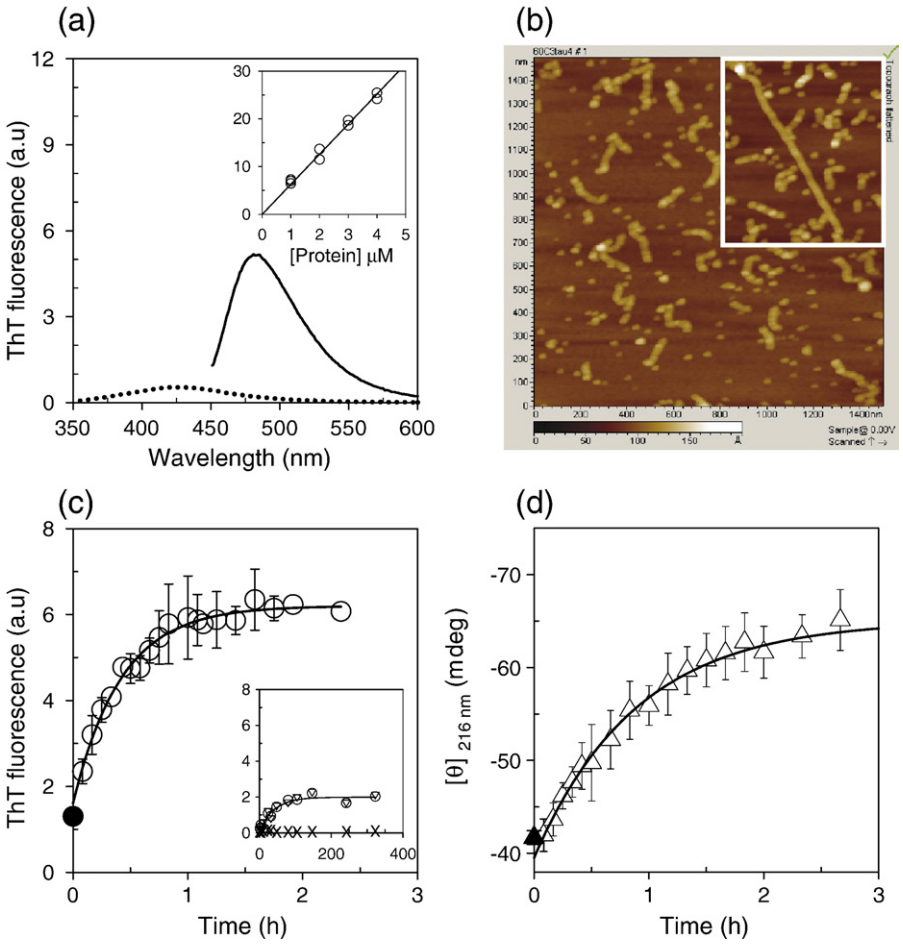

Figure 2. Formation of protofibrils at 60 °C. 50 μM protein was heated to 60 °C at pH 2.7. (a) Fluorescence emission spectra of 5 μM thioflavin T (ThT) in buffer alone (dotted line), and upon addition of protein to a final concentration of 1 μM from a sample of 50 μM barstar that had been heated to 60 °C at pH 2.7 for 3 h (continuous line). The inset shows the linear dependence of thioflavin T fluorescence (at 482 nm) on the concentration of protein present in the assay solution. The dye concentration was fixed at 5 μM, and the protein concentration varied between 1 μM and 4 μM. (b) An AFM image of the protofibrils formed by heating barstar to 60 °C at pH 2.7 for 3 h. The inset shows a sample that had been heated for 15 h and then incubated at 25 °C for 80 h, in which a straight amyloid fibril is also visible. The scale bar applies for the inset too. (c) Thioflavin T fluorescence-monitored kinetics at 60 °C (○). Inset: Thioflavin T fluorescence-monitored kinetics at 25 °C at pH 2.7 (○), at pH 2 (▽) and at pH 8 (×). (d) Ellipticity (at 216 nm)-monitored kinetics at 60 °C (Δ). In (c) and (d), the filled symbols represent the signal of the A form incubated for 6 h at pH 2.7, 25 °C, prior to heating. The continuous lines through the data in (c) and (d) are the least-squares fits to a single exponential equation. The error bars in (c) and (d) represent standard deviations from three separate experiments.

two probes is highly reproducible. This high reproducibility allowed the mean rate to be determined from measurements of the kinetic curves in three separate experiments. Mean rates and standard deviations so determined are shown in Figures 4 and 7.

Dynamic light scattering-monitored kinetics of the formation of amyloid protofibrils

The transformation of the A form into protofibrils is accompanied by an increase in the apparent hydrodynamic radii of the molecules. Figure 3(a) shows the change in the distribution of size in the population of protein molecules with time upon heating at 60 °C. It is seen that the increase in hydrodynamic radius is accompanied by an increase in the heterogeneity of the population, as indicated by the increase in the width of the distribution with time of heating. It is also evident that the distribution corresponding to that of the A form at 25 °C, disappears early during its transformation into protofibrils. From distributions such as that shown in Figure 3(a), it is possible to determine the mean apparent hydrodynamic radius as well as the total light scattering intensity as a function of time of heating. Figure 3(b) and (c) indicates that both the mean hydrodynamic radius and the total light scattering intensity increase in an exponential manner with the time of heating, and that no initial lag is seen in the change of either parameter. It is seen that the increase in mean hydrodynamic radius occurs significantly faster than that in the total light scattering inten-

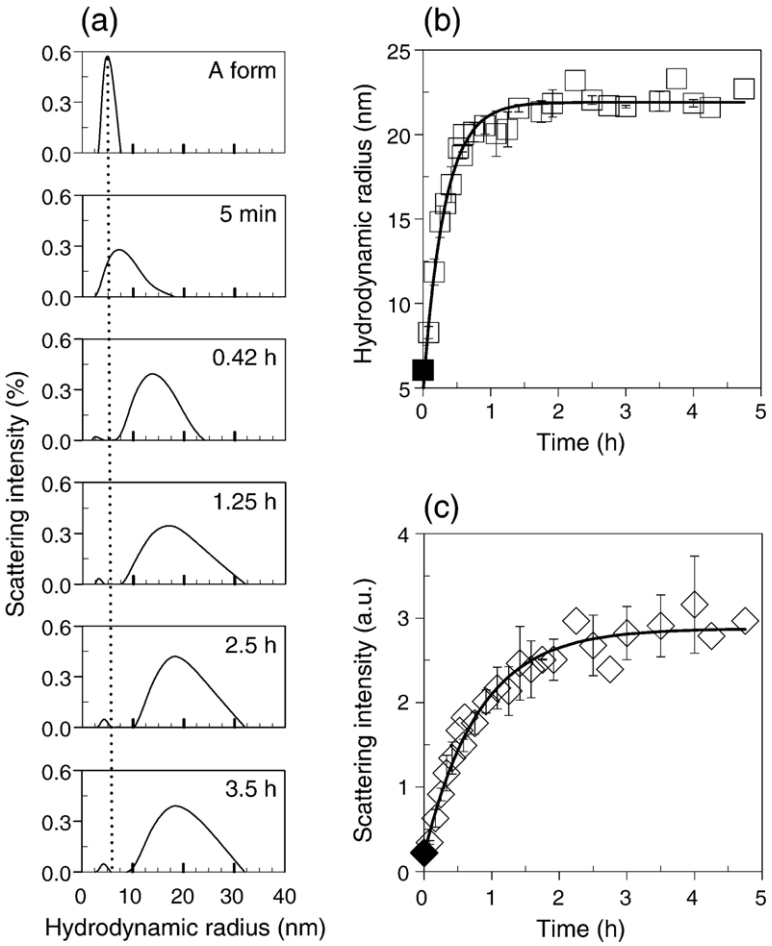

Figure 3. Kinetics of the formation of protofibrils at 60 °C monitored by DLS. 50 μM protein at pH 2.7 was heated at 60 °C. (a) The hydrodynamic radius distributions of the A form (soluble oligomers), and those at five different times of the aggregation at 60 °C, are shown. (b) Mean hydrodynamic radius-monitored kinetics (□). (c) Light scattering intensity-monitored kinetics (◊). In (b) and (c), the filled symbols represent the signal of A form at pH 2.7, 25 °C, prior to heating. The continuous-lines through the data in (b) and (c) are the least-squares fits to a single exponential equation. The error bars in (b) and (c) represent standard deviations from three separate experiments.

sity. Each data point in Figure 3(b) and (c) was highly reproducible, as indicated by the small error bars determined from three separate experiments; this allowed mean rates to be determined from the three experiments, which are shown in Figures 4 and 7.

Temperature dependence of the kinetics of amyloid protofibril formation

Figure 4 shows the kinetics of formation of protofibrils at four different temperatures, 40 °C, 50 °C, 60 °C and 70 °C, measured using four different probes, thioflavin T fluorescence, ellipticity at 216 nm, mean hydrodynamic radius, and light scattering intensity. It is seen that at all the temperatures and for all the probes, the kinetics are essentially those of a single-exponential process. For each probe and at each temperature, the single-exponential fit through the data points extrapolates back to the value of the signal determined for the A form at 25 °C (the species prior to heating). For all the probes, it is seen that the apparent rate of protofibril formation increases with an increase in temperature. It is also seen that the kinetic progress curves, except for the mean hydrodynamic radius-monitored curves, saturate at progressively higher values of the probe signal at higher temperatures.

In Figure 4(e), the apparent rate constants (k), obtained from the single exponential fits to the progress curves for protofibril formation (Figure 4(a)–(d)), are plotted against $1/T$. The slope obtained from such a linear Arrhenius plot gives the value of activation energy for the concerned process. For each probe, the Arrhenius plot is linear. The slopes of the Arrhenius plots, determined using different probes, are similar, even though the rate constants are dissimilar. The values of the activation energies, obtained with the different probes, are shown in the legend of Figure 4.

In Figure 4(f), the relative amplitude of the change in the probe signal (thioflavin T fluorescence, ellipticity at 216 nm, and light scattering intensity) is shown as a function of temperature. There appears to be, empirically, a linear relationship between the amplitude of signal change and temperature, and the dependence seems to be similar for each of the three probes. In contrast, the amplitude of the change in the mean apparent hydrodynamic radius is similar at all the four temperatures, that is, the final species formed at the four different temperatures all have the same mean apparent hydrodynamic radius (~20 nm).

Characterization of the amyloid protofibrils obtained at different temperatures

In Figure 5(a), it is seen that the far-UV CD spectra of the protofibrils obtained at three different temperatures are different from those obtained for the A form and for the native state. Whereas the spectra for the A form and the native state are more indicative of proteins containing significant α-helical secondary structure with peaks at 220 nm and 208 nm, the spectra for the protofibrils have a significant dip at 214–216 nm suggesting a higher β-sheet content. Protofibrils obtained at higher temperatures seem to have progressively higher mean residual ellipticity at 214–216 nm, suggesting that the β-sheet content increases with increasing temperature. The shapes of the spectra for the protofibrils formed at the three different temperatures are, however, similar. Such an increase in the mean residual ellipticity without a change in the shape of the spectra suggests either

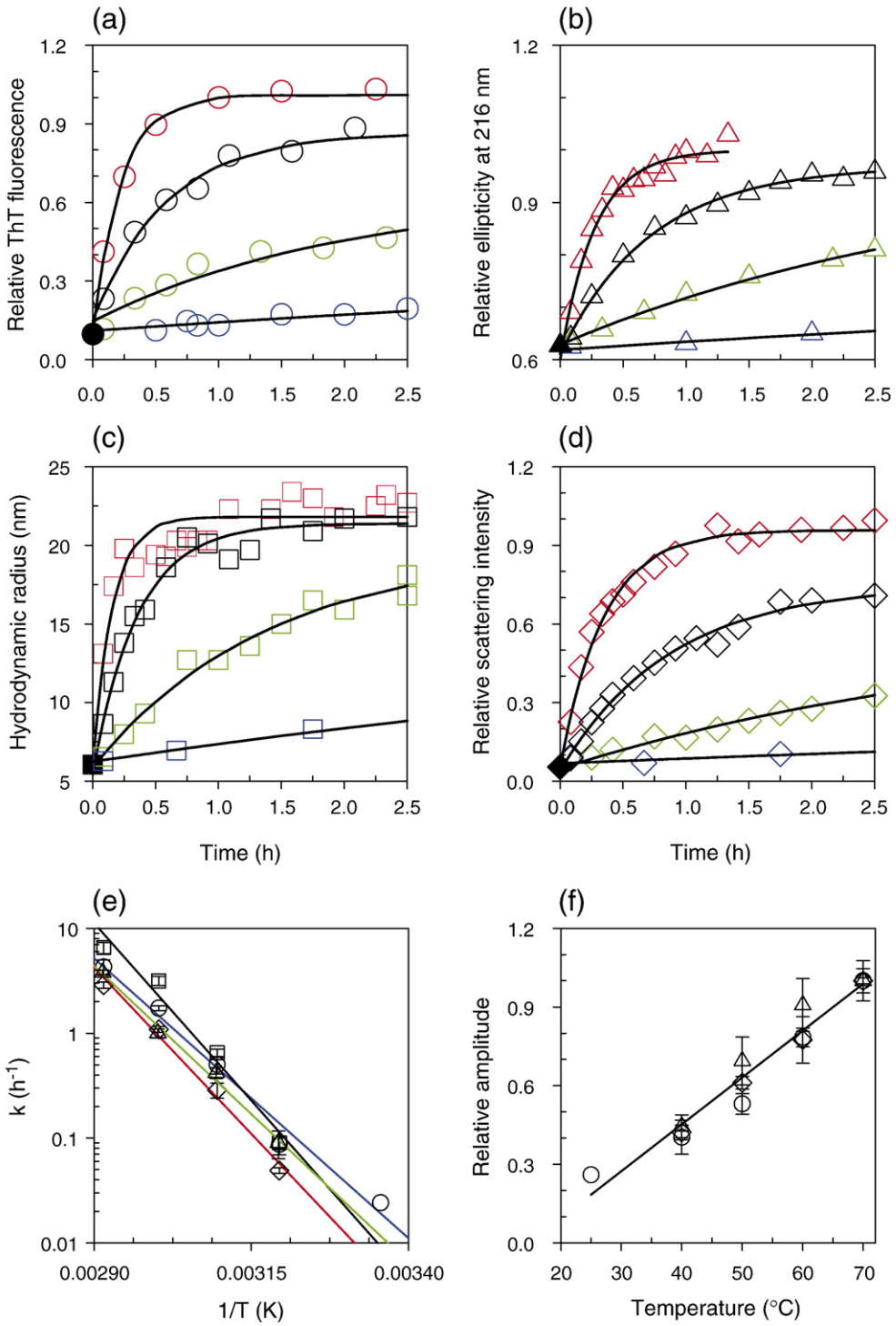

Figure 4 (*legend on next page*)

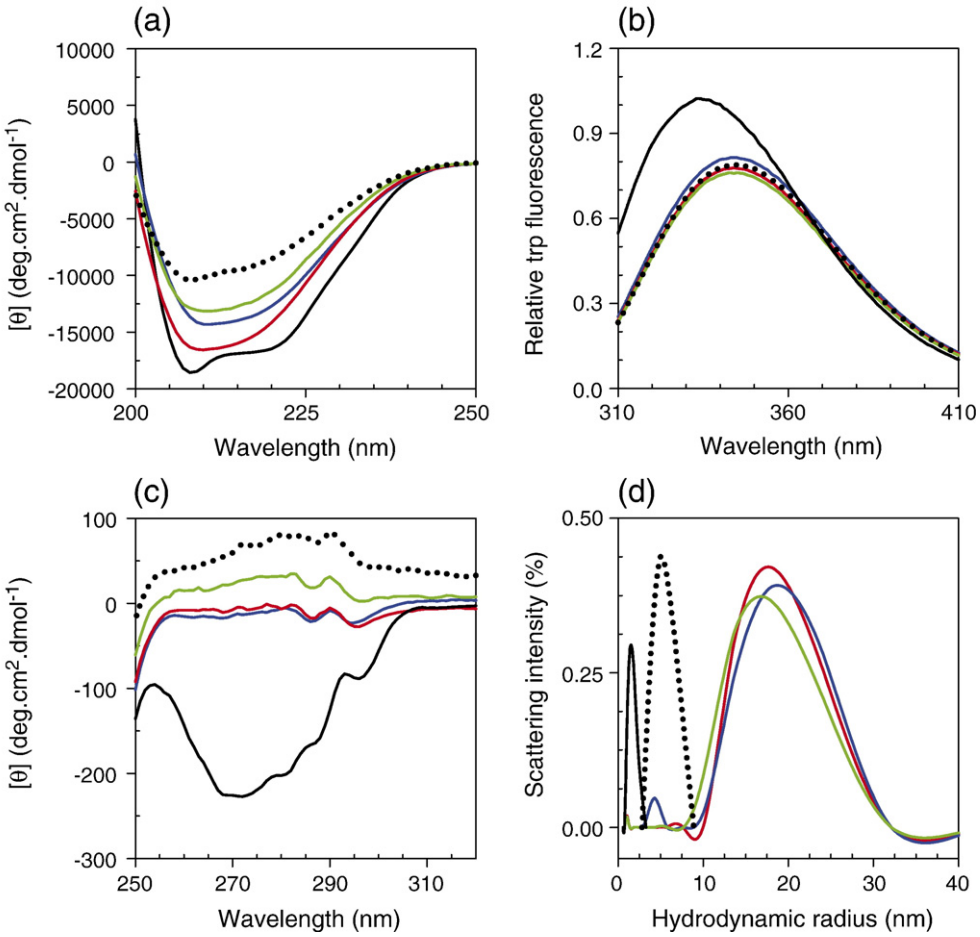

Figure 5. Characterization of the spectroscopic properties and size distributions of protofibrils formed at different temperatures. At each temperature, 50 μM protein at pH 2.7 was heated for a time corresponding to three time constants ($3/k$), where k is the apparent rate constant monitored by measurement of the ellipticity (at 216 nm). (a) Far-UV CD spectra. (b) Intrinsic Trp fluorescence spectra. (c) Near-UV CD spectra. (d) Apparent hydrodynamic radius distributions. In (b), the data are normalized relative to the fluorescence intensity of the native protein at 330 nm. In each panel, the green, blue and red lines represent data for the experiments carried at 50 °C, 60 °C and 70 °C, respectively. The dotted line represents the data for the A form at pH 2.7, 25 °C, immediately prior to heating, and the continuous black line represents the data for the native protein at pH 8, 25 °C.

that the protofibrils formed at the three temperatures are structurally different, or that progressively higher amounts of protofibrils are formed at higher temperatures.

In Figure 5(b), it is seen that the emission maximum of the intrinsic Trp fluorescence spectrum of the A form has a red shift of ~10 nm relative to that of the native protein. This shows that the three

Figure 4. Dependence on temperature of the kinetics of formation of protofibrils. 50 μM protein at pH 2.7 was heated to 40 °C (blue), 50 °C (green), 60 °C (black) and 70 °C (red). Representative data are shown for each probe. (a) Thioflavin T fluorescence-monitored kinetics at the four temperatures (○). (b) Ellipticity (at 216 nm)-monitored kinetics at the four temperatures (Δ). (c) Mean hydrodynamic radius-monitored kinetics at the four temperatures (□). (d) Light scattering intensity-monitored kinetics at the four temperatures (◊). In (a), (b), and (d), data at all the temperatures were normalized relative to the average $t=\infty$ signal for the corresponding 70 °C data. The filled symbols represent the signal of the A form at 25 °C, prior to heating. The continuous lines through the data are the least-squares fits to a single exponential equation. (e) Arrhenius plot: the observed rate constant, k, obtained from the fits in (a)–(d), is plotted against $1/T$. Linear fits through the data points (continuous lines) yield the following values for the activation energy: 102 kJ/mol for the thioflavin T fluorescence-monitored rate constants (blue line); 108 kJ/mol for the ellipticity (at 216 nm)-monitored rate constants (green line); 129 kJ/mol for the mean hydrodynamic radius-monitored rate constants (black line); and 121 kJ/mol for the light scattering intensity-monitored rate constants (red line). (f) The relative amplitude of the observed change in signal is plotted *versus* temperature. At each temperature and for each probe, the amplitude is determined as the change in signal from $t=0$ to $t=\infty$, and is normalized relative to the value of the amplitude observed for that probe at 70 °C. The continuous line represents a common linear fit through the three sets of data. In (e) and (f), the error bars represent standard deviations from three separate experiments.

Trp residues in the A form are in more unstructured environments than in the native state. It is also seen that the intrinsic Trp fluorescence spectra of the protofibrils obtained at the three different temperatures are similar and identical to the spectrum of the A form at 25 °C. It therefore appears that the three Trp residues in the protofibrils are as solvated as they are in the A form. In other words, the environments of the three Trp residues do not change in the transformation of the A form to protofibrils.

Figure 5(c) shows the near-UV CD spectra. The A form as well as the protofibrils have lost the characteristic spectrum of the native state, indicating that the aromatic residues in the A form and in the protofibrils are in unstructured environments.

Figure 5(d) compares the size distributions of the native protein, the A form, and the protofibrils. The distributions seen for the protofibrils are broader than the distribution seen for the A form, indicating a greater heterogeneity in the size of the protofibrils. But the protofibrils obtained at the three different temperatures appear to possess similar hydrodynamic radii and are equally heterogeneous in size.

These observations suggest that the protofibrils formed at the different temperatures cannot be distinguished by the spectroscopic and size characterization shown.

Dependence of the kinetics of amyloid protofibril formation on protein concentration

Figure 6 shows how the kinetics of conversion of the A form to protofibrils, at 60 °C, change with a change in protein concentration. For all the structural probes and at all the protein concentrations, the kinetics are well described as single-exponential. No lag in the kinetics is observed at any of the

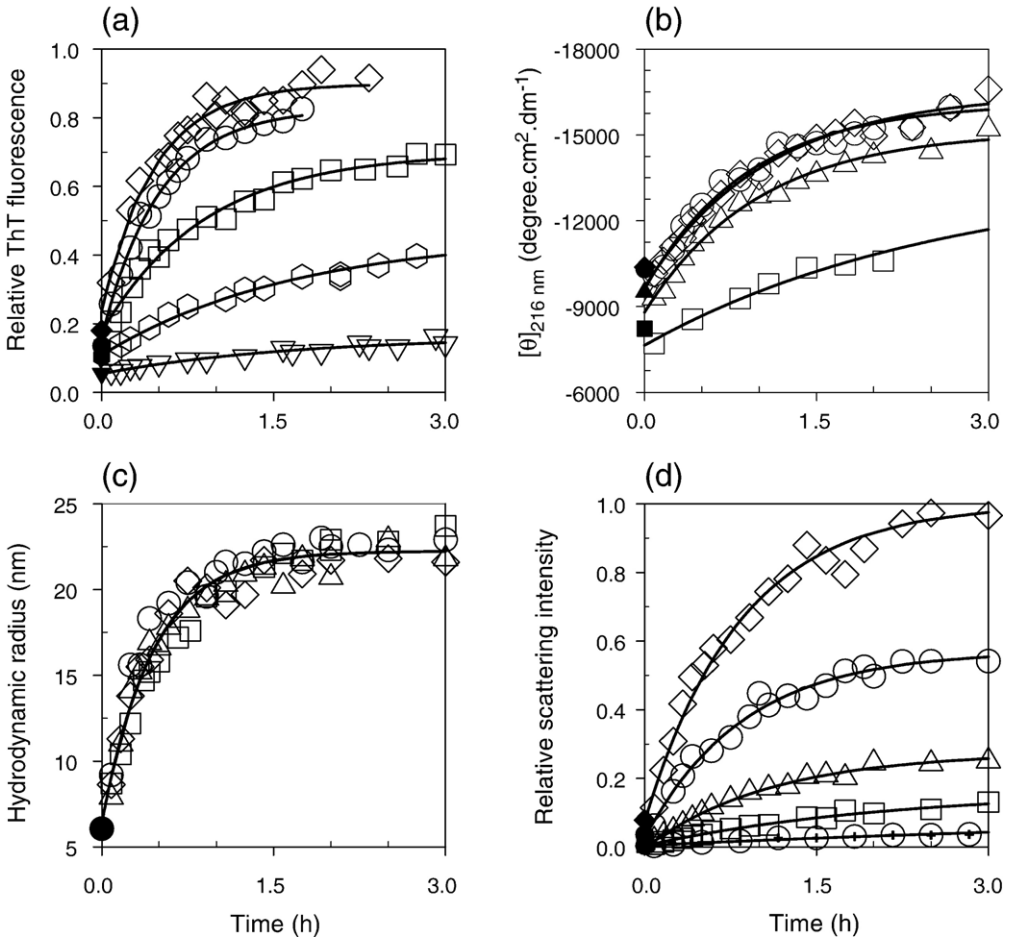

Figure 6. Dependence of the kinetics of formation of protofibrils, on protein concentration. Protein at pH 2.7 was heated to 60 °C. Representative kinetic traces are shown for each of the protein concentrations: 1 μM (▽), 2 μM (⬡), 2.5 μM (⊕), 5 μM (□), 10 μM (△), 25 μM (○), and 50 μM (◊). (a) Thioflavin T fluorescence-monitored kinetics: thioflavin T fluorescence is plotted against the time of aggregation. (b) Ellipticity-monitored kinetics: mean residue ellipticity at 216 nm is plotted against the time of aggregation. (c) Mean hydrodynamic radius-monitored kinetics: mean hydrodynamic radius is plotted against the time of aggregation. (d) Light scattering intensity-monitored kinetics: relative light scattering intensity is plotted against the time of aggregation. In (a) as well as (d), all data were normalized relative to the mean signal obtained for 50 μM protein at $t = \infty$. In all panels, the filled symbols represent the signals of the A form at 25 °C prior to the temperature jump, and the continuous lines through the data represent single-exponential fits. The values obtained for the apparent rate constants are shown in Figure 7.

protein concentrations, and for any of the structural probes used. All the kinetic traces of the signal change extrapolate at $t=0$ to the signal expected for the A form at the same protein concentration. When monitored by the change in thioflavin T fluorescence, the ellipticity at 216 nm, and the light scattering intensity, both the rate and the amplitude of signal change are seen to be dependent on the protein concentration (Figure 6(a), (b), and (d)). When monitored by the change in the mean apparent hydrodynamic radius (Figure 6(c)), it appears that a similar final value of the mean apparent hydrodynamic radius (~20 nm) is obtained at all the protein concentrations, and that the apparent rates determined are very similar. The data in Figure 6(c) indicate that the starting species for the formation of protofibrils at all the protein concentrations is the A form, which has a mean apparent hydrodynamic radius of 6 nm.

Figure 7(a) shows how the apparent rate constants for protofibril formation vary with a change in protein concentration. When monitored by the thioflavin T fluorescence assays in the protein concentration range of 1 μM to 50 μM, the apparent rate constant increases at low protein concentrations and then saturates at a protein concentration above 10 μM. When monitored by light scattering intensity measurements assays in the protein concentration range of 2.5 μM to 50 μM, a similar dependence of the apparent rate constant on protein concentration is observed. The minimum protein concentration that could be used for the ellipticity (at 216 nm) measurements was only 5 μM, and it seems that the dependences of the ellipticity and the light scattering intensity-monitored rate constants on the protein concentration fall on each other. Thioflavin T fluorescence, light scattering intensity and ellipticity at 216 nm yield similar dependences of the apparent rate constant on protein concentration in the range of 1 μM to 50 μM, with the apparent rate constant becoming independent of protein concentration at protein concentrations above 10 μM. It is also seen that the apparent rate constants monitored by light scattering intensity and ellipticity at 216 nm are virtually identical at each protein concentration. On the other hand, the apparent rate constant determined by measurement of the change in hydrodynamic radius has a very different dependence on protein concentration from the other three probes: it increases only marginally with an increase in the protein concentration range from 2.5 μM to 50 μM, and has an average value of 2.4(±0.5) h^{-1}. It would

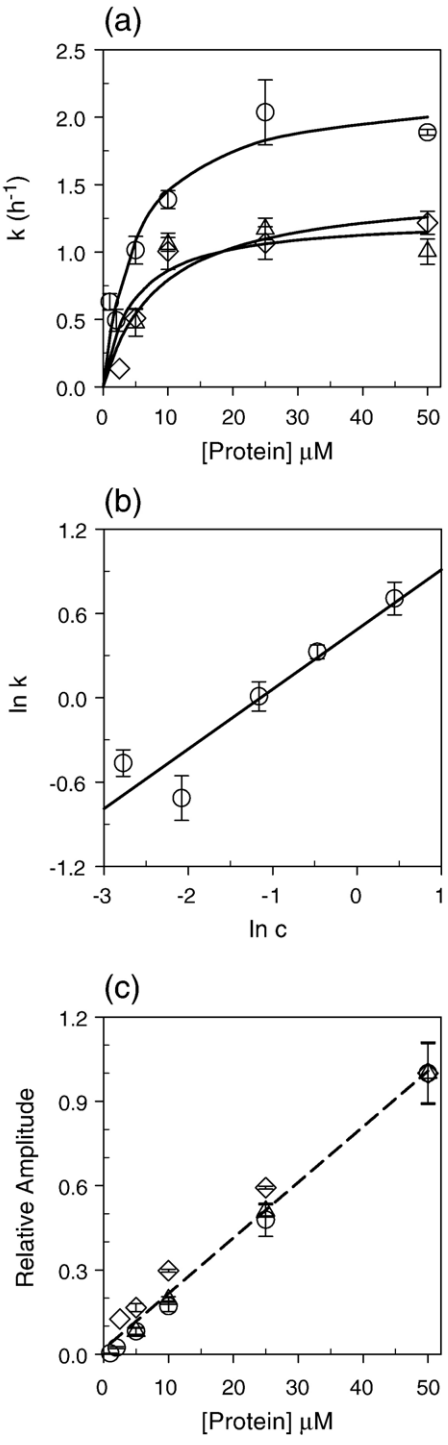

Figure 7. Dependence on protein concentration of the apparent rate constants and amplitudes of signal change associated with conversion of the A form to protofibrils. (○) Thioflavin T fluorescence-monitored kinetics; (△) ellipticity (at 216 nm)-monitored kinetics; (◊) light scattering intensity-monitored kinetics. (a) The apparent rate constants, obtained from Figure 6, are plotted against protein concentration. The continuous lines through the data are drawn by inspection only. (b) Plot of ln k against ln c, where k represents the rate constant for the transformation of the A form into protofibrils, monitored by measurement of the change in thioflavin T fluorescence, and c represents the concentration (in μM) of the A form. The continuous line represents a linear fit to the data points, and has a slope of 0.42. (c) The total amplitude of the signal change obtained for each probe at each protein concentration was determined as the difference in the signals at $t=0$ and at $t=\infty$. For each probe, the amplitudes are normalized relative to the average amplitude observed for that probe at 50 μM protein concentration. The broken line is a common linear fit to all three sets of data. In all the three panels, the error bars represent standard deviations determined from three separate experiments.

appear that the hydrodynamic radius-monitored apparent rate constant has reached its saturating value at a lower concentration (~2.5 μM) than that at which the apparent rate constants measured by the other probes saturate.

All probes yield an apparent rate constant that is only weakly dependent on protein concentration. To better expose the weak dependence on protein concentration of the rate constant of aggregation, the logarithm of the apparent rate constant determined by the thioflavin T fluorescence assay, is plotted against the logarithm of the protein concentration in Figure 7(b). The slope of a linear fit to the data in such a plot, is determined to be only 0.42.

Figure 7(c) compares the dependence on protein concentration of the amplitude of signal change during the transition of the A form to protofibrils, for the different structural probes. The changes in thioflavin T fluorescence upon binding, ellipticity at 216 nm, and the light scattering intensity, appear to show a similar linear dependence on protein concentration. On the other hand, the amplitude of change in the mean apparent hydrodynamic radius seems to be independent of protein concentration (Figure 6(c)): at all the protein concentrations, protofibrils of similar mean apparent hydrodynamic radius (~20 nm) are formed.

Disaggregation of amyloid protofibrils at pH 8

Figure 8 shows that on transferring protofibrils (formed by heating protein at 60 °C for 3 h at pH 2.7) from pH 2.7 to pH 8 at 25 °C, the protofibrils are no longer stable and they disaggregate. The amount of protofibrils, as determined by their ability to bind to thioflavin T and enhance its fluorescence, reduces with the time of incubation at 25 °C (Figure 8(a)). After an incubation of the protofibrils at pH 8 for 60 h, there is virtually no thioflavin T binding capacity left. The kinetics of decrease in the thioflavin T fluorescence are well-described as three-exponential, which suggests that the process of disaggregation happens in three steps. When a similar assay is used to monitor disaggregation of the A form to native protein at pH 8, the weak thioflavin T binding ability of the A form was found to disappear much faster, within 3 min (Figure 8(a), inset). The absence of a 3 min kinetic phase in the disappearance of thioflavin binding ability during the disaggregation of protofibrils (Figure 8(a), inset), indicates that no A form is present after 3 h of heating at 60 °C, pH 2.7. Even when protein was heated at 60 °C, pH 2.7 for only 1 h, no A form could be detected (data not shown).

To determine whether the protofibrils have transformed to native protein after prolonged incubation at pH 8, the intrinsic Trp fluorescence spectrum, the far-UV CD spectrum and the gel filtration chromatogram of the protein were determined at an incubation of 100 h at 25 °C after the pH jump from pH2.7 to 8. Figure 8(b), (c) and (d) shows that the intrinsic Trp fluorescence and far-UV CD spectra, as well as the gel filtration chromatogram, of the disaggregated protein are identical to those of native protein that had first been heated at 60 °C for 3 h at pH 8, and then been incubated for 100 h at 25 °C, pH 8. Hence, it appears that the product of protofibil disaggregation at pH 8 is native barstar.

Discussion

In this study, multiple structural probes of protein conformation were used in an attempt to delineate the steps involved in the formation of amyloid protofibrils from a specific soluble oligomer (the A form) of the small protein barstar, which is formed at low pH. These probes include thioflavin T fluorescence, ellipticity at 216 nm, apparent hydrodynamic radius, and light scattering intensity. Multiple structural probes are needed for proper characterization of any protein aggregation process because of the high heterogeneity inherent in it. It is expected that the use of multiple structural probes will ultimately provide as much insight into the nature of protein aggregation, as it has in the study of protein folding, another reaction where a polypeptide chain self-assembles into a specific structure.[50]

How similar are protofibrils formed at different temperatures?

It is seen that the changes in thioflavin T binding capacity, ellipticity at 216 nm, and light scattering intensity, upon protofibril formation, scale similarly with the temperature at which protofibril formation is induced (Figure 4(f)). This result might suggest that different amounts of the same type of protofibril are formed at the different temperatures. But this would imply that at the lower temperatures, a certain fraction of the protein is not competent to form protofibril, because of an unknown kinetic barrier, and this fraction decreases with increasing temperature. It is clear that the fraction that has not transformed to protofibrils at the time the observed kinetic process has completed, has not remained as the A form: the A form disappears relatively early during the aggregation process (Figure 3(a)). Moreover, when the disaggregation assay (Figure 8) is carried out at an early time of aggregation, it is not possible to detect any species that can transform to native protein at pH 8 at the same apparent rate with which the A form transforms to native protein. Thus, the fraction that has not transformed to protofibrils does not appear to remain as the A form or in an aggregate with the same size as that of the A form, but would nevertheless have to be present in a form whose secondary structure and thioflavin T binding capacity are similar to those of the A form.

An alternative explanation for the observation of increasing signal change in thioflavin T binding capacity, ellipticity at 216 nm and light scattering intensity, during protofibril formation at increasing temperature is that all the protein is transformed to protofibrils at the different temperatures, but the

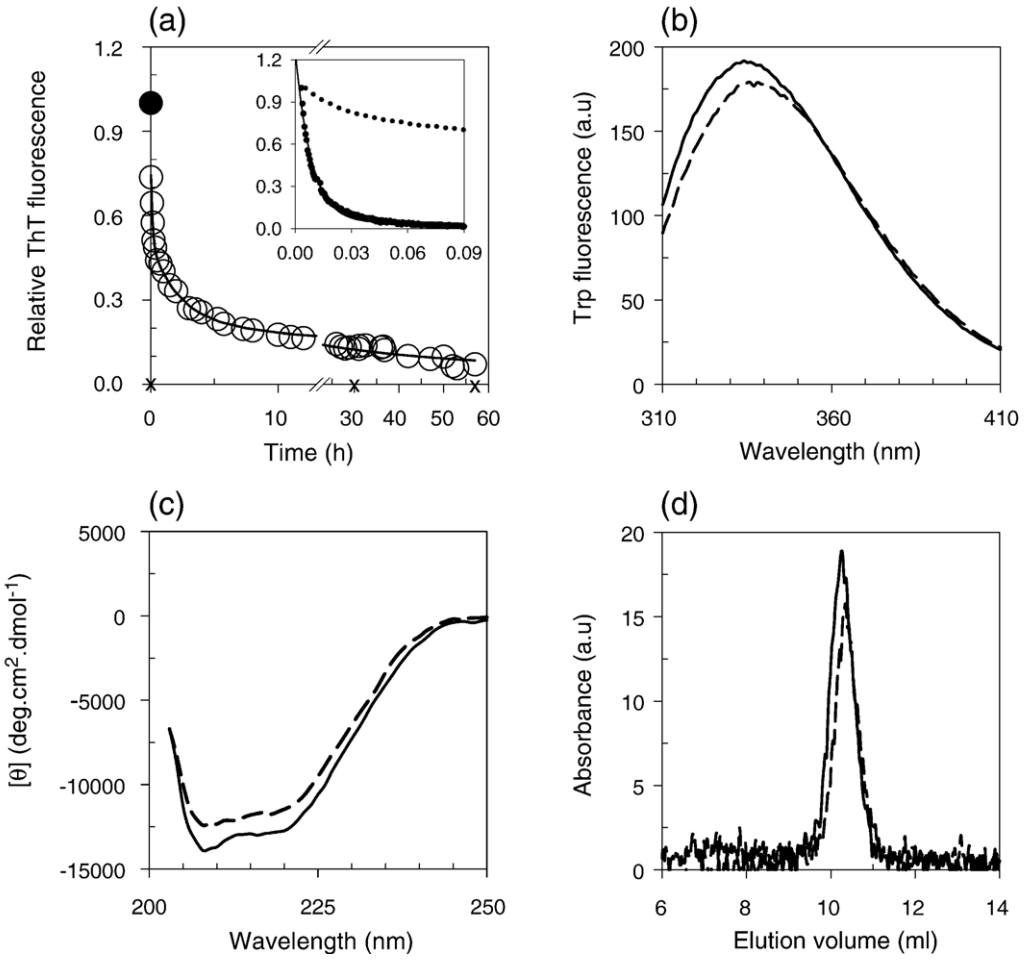

Figure 8. Disaggregation of amyloid protofibrils at pH 8, 25 °C. Protofibrils obtained after 3 h of incubation of 10 μM protein at pH 2.7, 60 °C were shifted into pH 8 buffer. (a) Kinetics of disaggregation. Thioflavin T fluorescence assays were carried out at different times after the change in pH of the protofibril solution from pH 2.7 to 8. Open circles represent the kinetic data points for the disaggregation. The filled circle shows the thioflavin T fluorescence before the pH jump to pH8, and the crosses show the thioflavin T fluorescence for native protein at pH 8. The thioflavin T fluorescence is plotted against the time of incubation at pH 8. The data are normalized relative to the thioflavin T fluorescence before the pH jump to pH8. The continuous line through the data is a three-exponential fit which yields apparent rate constants for disaggregation of 7.7 h^{-1}, 0.46 h^{-1} and 0.03 h^{-1}. The inset shows the kinetics of conversion of the A form to native protein (●), monitored by the disappearance of thioflavin T binding ability of the A form after a jump in pH from pH 2.7 to 8. The continuous line through the data (●) is a single exponential fit which yields an apparent rate constant for conversion of the A form to native protein of 115 h^{-1}. The dotted line in the inset is the kinetic trace of disaggregation of the protofibrils at pH 8, which was determined by monitoring the decrease in fluorescence of thioflavin T, when disaggregation was carried out in the presence of the dye. (b) Intrinsic Trp fluorescence spectrum of disaggregated protein at pH 8. (c) Far-UV CD spectrum of disaggregated protein at pH 8. (d) Gel filtration profile of disaggregated protein at pH 8. In (b), (c), and (d), broken lines represent the disaggregated sample at 100 h of incubation at pH 8, 25 °C, and the continuous lines represent native protein that had also been heated at 10 μM for 3 h at pH 8, 60 °C.

protofibrils formed at the different temperatures have different structures. For example, the extent of secondary structure and the number of thioflavin T binding sites present could be different in the protofibrils formed at the different temperatures. Nevertheless, the protofibrils formed at the different temperatures have the same apparent hydrodynamic radius (Figure 5(d)). Both theoretical and experimental studies have shown that a twofold increase in the diameter of a cylinder (rod) of a given length leads to only an 1.3-fold increase in hydrodynamic radius.[51,52] Since protofibrils are rod-like, it is possible for protofibrils formed at the different temperatures to have the same apparent hydrodynamic radius but have different diameters (widths)[53] provided that they are not too long, as is the case here. Protofibrils of the same apparent hydrodynamic radius will have different widths if they occur in multi-stranded forms. It is possible that protofibrils formed at higher temperatures are multi-stranded because of lateral association of linear aggregates (see below). The presence of multi-stranded protofibrils at the higher temperatures would account for the higher light scattering intensities seen for the protofibrils formed at the higher temperatures.

The A form transforms directly into protofibrils

The use of multiple structural probes in this study suggests that the 16-mer A form transforms directly into protofibrils. For each probe and at each temperature, the kinetics appear to be well-described as single exponential, and the exponential fit to the kinetic data points extrapolates, at time $t=0$, to the value of the signal determined for the A form (Figure 4(a)–(d)). Since the probes include measures of secondary structure (ellipticity at 216 nm), size (apparent hydrodynamic radius), total aggregated material (light scattering intensity), as well as specific fibrillar structure (thioflavin T binding capacity), this is strongly indicative of the A form being a direct structural precursor of the protofibrils. A previous study, based on mapping residue-specific side-chain dynamics in the A form and in the protofibrils, had in fact, suggested that the A form of barstar transforms directly into protofibrils.[13] Even though the side-chain dynamics were found to be dampened more in the protofibrils than in the A form at all residue positions, the pattern remained the same in both. It seems quite unlikely that the A form would dissociate, and the smaller oligomers would then re-associate to form protofibrils with an internal structure so similar to that of the A form.

Protofibril formation does not show the characteristics of nucleation dependent polymerization

It could be expected that the process of protofibril formation, which involves aggregation of smaller protein units, might occur though a nucleation dependent polymerization mechanism,[54–57] analogous to the mechanism involved in the crystallization of proteins.[58] But the transformation of the A form to protofibrils, does not display any of the characteristics of nucleation dependent polymerization.[57] The kinetics of protofibril formation do not display a weak start (lag phase) in the initial part of the reaction, over a 50-fold range of protein concentration (Figure 6). The time course of the reaction, for each probe and at each protein concentration, is well described as single exponential. The dependence of the amplitude of change in the signal on protein concentration (Figure 7(c)) shows that there is apparently no critical concentration barrier for the process, as expected for nucleation dependent aggregation. Finally, the observed rate of formation of protofibrils, monitored by either of the four probes, has a very weak dependence on protein concentration (Figure 7(a)). A plot of ln k *versus* ln c, for the thioflavin T fluorescence-monitored kinetics, suggests that the aggregating nucleus would have to be monomeric (the same size as the A form) (Figure 7(b)). This could mean that if a nucleation event does occur, it would have to be a folding event, as it appears to be in the case of poly(Gln) aggregation.[59] Given the lack of a lag phase, and other prominent features of nucleation-dependent polymerization, as discussed above, this is unlikely in the case of barstar aggregation.

A protein concentration-independent transition occurs during transformation of the A form into protofibrils

The observation that the apparent rate constant for protofibril formation does not keep increasing with increasing protein concentration, but instead becomes independent of protein concentration at protein concentrations greater than 10 μM (Figure 7(a)), does suggest, however, that the process of protofibril formation involves a structural transition which is independent of protein concentration. Such a protein concentration-independent transition could, for example, be a conformational conversion transition late during the aggregation process. For example, if a slow conformational conversion were to occur in critically sized aggregates consequent to protein concentration-dependent association steps, it could become the rate-limiting step at high protein concentrations (>10 μM) where the association steps become faster.

An alternative explanation for why the kinetics of the conversion of the A form to protofibrils become independent of protein concentration at high protein concentrations could be that the 16-mer A form dissociates into smaller A forms in the protein concentrations of 1 μM to 10 μM. If only the 16-mer A form were the aggregation competent form, as appears to be the case (see above), in other words if the smaller A forms were off-pathway, then the concentration-dependence of the overall aggregation process could reflect the protein concentration-dependence of the re-association of the smaller A forms into the 16-mer A form. Such an explanation is unlikely because (1) there is no evidence so far of the A form dissociating at low protein concentration; (2) the dependence on protein concentration of the apparent rate of protofibril formation would be expected to be much stronger than the weak dependence, which is observed (Figure 7(a) and (b)) unless the smaller off-pathway A form were only an 8-mer, and not a monomer, dimer or tetramer; and (3) the rate of aggregation would increase with increasing protein concentration, and not saturate at concentrations greater than that at which all protein is associated in the 16-mer A form, as is observed. Regardless of whether a conformational transition becomes rate limiting at protein concentrations greater than 10 μM, it is necessary to understand the probe-dependent kinetics of protofibril formation.

Transformation of the A form into protofibrils occurs in many steps

The different probes each yield a different apparent rate of protofibril formation (Figures 4 and 7), although the apparent rates measured by the change in ellipticity at 216 nm and by the change in total scattering intensity being virtually

identical (Figure 7(a)). The differences in rates measured using different probes suggest multiple steps in the aggregation process. In particular, the difference in the dependence on protein concentration of the rate constant measured by change in apparent hydrodynamic radius and by the change in scattering intensity (Figure 7(a); see Results) suggests strongly that the two probes are measuring different steps in the process of protofibril formation. The apparent hydrodynamic radius grows the fastest. This measure is biased towards the largest aggregates present at any time, and is not proportional to the total amount of aggregate that is present. Hence, it is not surprising that the apparent rate measured by the change in apparent hydrodynamic radius, does not change with protein concentration. The increase in thioflavin T binding capacity monitored by fluorescence, and the increase in secondary structure monitored by far-UV CD, both reflect specific conformation conversion within the aggregates, and both measures are proportional to the total amount of aggregate present. It appears that the specific structural changes leading to the formation of thioflavin T binding sites, precedes the specific changes in secondary structure. The increase in light scattering intensity, which also depends on the amount of aggregate, occurs at the same apparent rate as the rate of the increase in β-sheet secondary structure (Figure 7(a)). As expected, all three probes for which the signal is proportional to the amount of aggregate present, namely thioflavin T fluorescence, ellipticity at 216 nm, and light scattering intensity, yield similar dependences of the apparent rate constant of protofibril formation on protein concentration.

Although the differences in apparent rates determined using different probes are larger at higher temperatures, the activation energies determined for the various steps are somewhat similar in value (Figure 4). This is surprising because different steps in the aggregation process would normally be expected to have different activation energies. It is possible that the different steps of the aggregation process have similar activation energies because they are all complex association events. There are other possible explanations: each step in the aggregation process could be tightly coupled to a conformational change with an activation energy of ~100 kJ/mol, or more likely, such a conformational change occurs concomitantly with and independently of the aggregation steps during protofibril formation.

What could such a conformational change be? The large activation energy (~100 kJ/mol) associated with the conversion of the A form into protofibrils (Figure 4) might originate from the *trans* to *cis* isomerization reaction of the Tyr47–Pro48 peptide bond, assuming such an isomerization reaction occurs during protofibril formation, as it does during the folding of the protein to its native state.[50] It is quite remarkable that the activation energy for protofibril formation is so similar in value to that measured earlier for the folding reaction. It could mean that the overall rate of protofibril formation by barstar might be limited by proline isomerization, as is the overall rate of barstar folding. Future experiments will be targeted towards better understanding the contribution of the proline isomerization reaction during the aggregation process.

Lateral association of aggregates occurs concurrently with conformational conversion

The intensity of light scattered by an aggregate in solution is proportional to the second power of the aggregate mass,[53] and also to the number of aggregate particles. Hence, the slow change in light scattering intensity, which occurs as the slowest step during protofibril formation, must indicate an increase in either the mass of the aggregate or in the number of aggregate particles. At high protein concentration, the number of aggregating particles cannot be increasing, because then the apparent rate, measured by light scattering intensity, would depend on protein concentration, which it is not. Thus, the increase in light scattering intensity must reflect an increase in the average mass per aggregate. This increase in aggregate mass is not reflected in an increase in the apparent hydrodynamic radius (Figures 5 and 6), suggesting that the aggregate mass does not increase by linear aggregation that is by an increase in the length of the aggregate. The only way that aggregate mass can increase, leading to an increase in light scattering intensity, without a concomitant increase in apparent hydrodynamic radius, is if the mass increases by lateral association of already formed aggregates (see above). For example if two linear aggregates of equal mass were to associate laterally, the number of aggregate particles would halve, but the mass of each aggregate would double, and the light scattering intensity would be twice than that before lateral association. During the process of protofibril formation by the Dutch variant of amyloid β, light scattering intensity was observed to increase after the apparent hydrodynamic radius had stopped increasing. Such behavior had been attributed to lateral association,[53] and is similar to that seen for barstar (Figure 3(b) and (c)).

The apparent rate of lateral association of aggregates would normally be expected to increase with increasing protein concentration. But at high protein concentrations (>10 μM), the apparent rate measured by monitoring light scattering intensity is seen to be independent of protein concentration (Figure 7(a)). This can only be possible if lateral association involves two steps: a fast step that is the protein concentration-dependent encounter step, and a slower step involving a protein concentration-independent conformational transition within the encounter complex. The observation that the apparent rate constant of the change in light scattering intensity occurs at the same rate as that of the change in ellipticity at 216 nm, at all protein concentrations (Figure 7(a)), suggests that

the slow protein concentration-independent component of lateral association is the slow step in conformational conversion, namely the increase in β-sheet structure (see above).

Multiple routes exist for the formation of protofibrils

It is important to ask whether the different steps in protofibril formation, which have been identified by the use of the different structural probes, occur on only one or on multiple pathways of aggregation. The absence of a lag phase in the observed kinetics of change in far-UV circular dichroism or in light scattering intensity, which occur the slowest, suggest that the changes in these parameters must be occurring in parallel with and independent of, the faster changes in thioflavin T binding capacity. In other words, it appears that there must be multiple pathways for aggregation from the A form to the protofibrils. Given the heterogeneity in size of the A form and the even greater heterogeneity in size of the protofibrils (Figure 3(a)), as well as the seemingly progressive nature of the transformation from the former to the latter (Figure 3), it is not surprising that the transformation occurs along multiple routes. The observation that the same activation energy for protofibril formation is measured by the four different probes also suggests that each of the probes reports on the activation energy averaged over multiple pathways because a change in each probe signal must necessarily occur along each pathway.

Protofibril formation appears to proceed *via* association of higher oligomeric intermediates

One possible mechanism for the formation of protofibrils from the A form is that growth of the aggregate occurs through the sequential addition of A form oligomers. Such a mechanism requires that the A form be present throughout the aggregation process. As discussed above, the A form cannot be detected at early times of the aggregation process, either in a study of the evolution of the distribution of the apparent hydrodynamic radius with the time of heating (Figure 3(a)), or in a study of the disaggregation of aggregated forms at an early time of aggregation (Figure 8, and data not shown). It therefore appears that the A form assembles into higher order aggregates early during the transformation process, and that these higher-order aggregates then assemble further in a progressive manner. At later stages of the aggregation process, once aggregates of a critical size, with an apparent hydrodynamic radius of ~20 nm, have developed, it appears that further growth occurs through lateral association of these critical aggregates, finally leading to the formation of protofibrils. Specific structural changes within the aggregates, reflected in an increase in the number of thioflavin T binding sites and an increase in β-sheet structure, appear to occur only at the time of lateral association.

This model of progressive aggregation (Figure 9) predicts that the distribution of sizes should become unimodal at an early time of aggregation and that it should then change in a continuous manner thereafter. This is observed (Figure 3(a)). The model predicts that the changes in thioflavin T binding capacity and far-UV circular dichroism will saturate only after the final size is reached because the specific structure responsible for these changes, manifests itself only after a particular aggregate size (apparent hydrodynamic radius) is attained. This too is observed (Figure 4). The model predicts that these changes in specific structure will occur along with the slow change in light scattering intensity, which reports on the lateral association of large critical aggregates in which the specific structural changes have already manifested themselves.

Such a model of progressive aggregation and late association of large critical aggregates leading to protofibril formation, which has been observed here for barstar appears to be quite similar to processes of cluster-cluster aggregation,[60,61] where aggregates of different sizes can associate with one another. The mechanism appears to be shared by several proteins including the yeast prion protein Sup35,[19,62] amyloid β protein,[20,63,64] yeast phosphoglycerate kinase[65] and transthyretin.[66] It therefore appears that the processes of amyloid protofibril formation from different proteins share the common feature of having oligomeric intermediates as the units of association. The conversion of single-stranded amyloid protofibrils to multi-stranded ones by lateral association may be an important step in their conversion to amyloid fibrils, because multi-stranded filaments can grow to much longer lengths than can single-stranded ones.[67]

Finally, it is useful to summarize the results presented here on the process of protofibril formation by barstar, by alluding to the remarkable similarity between the fibrillization of barstar and that of amyloid β protein.[68] In both cases, protofibril formation commences from 4–6 nm spherical aggregates, which might be micellar-like,[20,41,42] and which are molten globule-like.[25,38,39] As in the case of barstar, so also for amyloid β protein, no lag phase is observed and protofibril formation occurs non-cooperatively,[64] the activation energy for protofibril formation is around 23–25 kcal/mol,[69] and the apparent rate of protofibril formation saturates at higher protein concentrations.[20] For amyloid β protein too, there is some evidence for lateral association in the growth of the protofibrils,[63] and the final protofibrils have the same apparent hydrodynamic radius of 20 nm[20] as do those of barstar. From this study, it appears that the aggregation of barstar occurs *via* multiple steps along multiple routes, and that lateral association of critically sized aggregates is coupled to conformational conversion. It is likely that these results are also true in the case of amyloid β protein. Not only do amyloid protofibrils[70] of different proteins share common structural features, as do amyloid fibrils,[71]

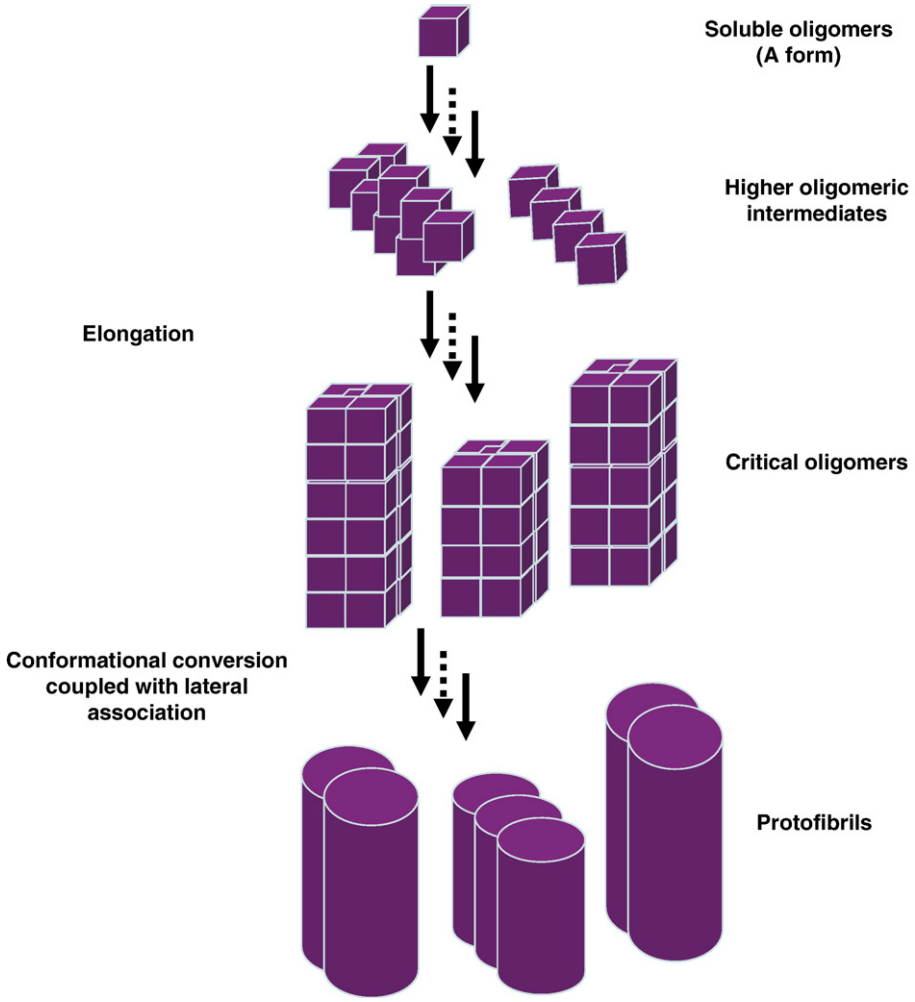

Figure 9. Schematic model for the formation of amyloid protofibrils from the A form. Conversion occurs in multiple steps. The A form, which is a micelle-like and molten globule-like 16-mer, is first converted into an amyloidogenic aggregate. Extension into single-stranded aggregates of a critical size (up to 20 nm in apparent hydrodynamic radius) then occurs. Finally, lateral association leading to the formation of multi-stranded protofibrils occurs, concurrently with specific structural changes that lead to the formation of thioflavin T binding sites and specific secondary structure indicative of β-sheet. Multiple kinetic routes operate from the A form to the protofibrils.

but it seems that the mechanism by which protofibrils form may also be conserved.

Materials and Methods

Protein expression and purification

Wild-type barstar was expressed and purified using the procedure described.[38] The purity of the protein was confirmed by SDS–PAGE and by mass spectrometry using a Micromass Q-TOF Ultima spectrometer, and was found to be more than 98% pure. The mass of the protein as determined by mass spectrometry was 10,342 Da.

Buffers, solutions and experimental conditions

All reagents used to make buffers were of the highest purity grade available from Sigma. The protein was dissolved initially in 20 mM Tris buffer (pH 8). This was diluted tenfold into 50 mM glycine buffer (pH 2.7). All the buffers contained 1 mM DTT, except for the CD measurements and the disaggregation study, where they contained 200 μM DTT. The protein concentration used for most of the experiments was 50 μM, except for the concentration dependence studies where it was varied between 1 μM and 50 μM and for the disaggregation study where it was 10 μM. The protein concentration was determined by measuring the absorbance at 280 nm, using $\varepsilon_{280} = 23{,}000\ M^{-1}\ cm^{-1}$.

Aggregation studies

The aggregation process was monitored by fluorescence, CD and dynamic light scattering (DLS) measurements on three different instruments each with its own temperature control system. In order to avoid any artifact arising from the use of different temperature control systems on these different instruments, as well as from the use of different size cuvettes for these measurements, the aggregation process at each elevated temperature was carried out in a heating block. Samples were first incubated for 6 h at pH 2.7, 25 °C, and then transferred

to the heating block set at the desired final temperature (40(±0.5) °C to 70(±0.5) °C). The same heating block was used for all measurements with all probes. In all the cases, the final temperature was reached within 5 min of the transfer of the sample to the heating block. At different times of incubation at the desired temperature, aliquots of the samples were withdrawn for analysis by the thioflavin T fluorescence assay, fluorescence or circular dichroism spectroscopy, or by dynamic light scattering. All these measurements were done after first cooling the withdrawn aliquots to 25 °C within 4 min. All samples for all measurements using the different probes were handled in as similar a manner as possible.

Thioflavin T fluorescence assay

For the assay, a calculated amount of protein was withdrawn from the heated sample, cooled to 25 °C, and then added to the assay solution (containing thioflavin T), so that the final protein and dye concentrations in the assay solution were 1 μM and 5 μM, respectively. In the assay solution, the pH was adjusted to pH 8, by appropriate mixing of 50 mM Tris buffer (pH 8.65) and 50 mM glycine buffer (pH 2.7) with the sample aliquot. When protofibril formation was carried out using 1 μM protein, the protein and dye concentrations in the assay solution were 0.5 μM and 2.5 μM, respectively. The final pH of the assay solution was 8. Thioflavin T fluorescence was measured within half a minute of addition of the protein to the assay solution. The dye fluorescence decreased less than 10% during this time. The measurements were carried out on a Fluoromax-3 spectrofluorimeter (Jobin Yvon) by exciting the sample at 440 nm and by monitoring the emission at 482 nm. The excitation and emission slit widths were set at 1 nm and 10 nm, respectively. The emission spectra of 5 μM free thioflavin T, and that with 1 μM protein were collected with the excitation wavelengths at 342 nm and 440 nm, respectively. The excitation and emission slit widths were 1 nm and 10 nm, respectively.

Spectroscopic measurements

Far and near-UV CD measurements were carried out using a Jasco J-720 spectropolarimeter, and cuvettes of 0.5 mm and 10 mm path-length, respectively. Spectra were collected in the 195 nm–250 nm and 250 nm–320 nm range, with a step resolution of 1 nm, a scan speed of 100 nm/min and a bandwidth of 1 nm. Each spectrum was averaged over 50 scans. For the kinetic studies, the ellipticity at 216 nm was monitored at regular intervals.

The intrinsic Trp fluorescence emission spectra were recorded on a Fluoromax-3 spectrofluorimeter by exciting the samples at 295 nm. The excitation and emission slit widths were set at 0.5 nm and 10 nm, respectively. Each spectrum was averaged over five scans.

Dynamic light scattering measurements

The DLS experiments were carried out using a DynaPro-99 unit (Protein Solutions Ltd). All the buffers and the pH 8 protein solutions were filtered through a 0.02 μm filter (Whatman Anodisc 13), and were spun at 10,000 rpm for 20 min, before addition of protein. All the centrifuge tubes, used in the experiments, were rinsed twice with 0.22 μm filtered buffer, and then twice with buffer filtered through a 0.02 μm filter. The pH jump was given into a 50 mM glycine solution (pH 2.7) containing 1 mM DTT, with the help of tips rinsed several times with the filtered glycine buffer. The samples were incubated at 25 °C for 6 h before the temperature jump. After the temperature jump in the heating block, aliquots were withdrawn at regular intervals and cooled to 25 °C. The cooled aliquot was put into a 45 μl cuvette, and then the cuvette was placed in the sample chamber maintained at 25 °C. The sample was illuminated with a laser of wavelength 829.4 nm. The scattering intensity at 90°, and its autocorrelation function were measured simultaneously. For each time point, 20 acquisitions were collected. The instrumental settings used were as follows: acquisition time, 5 s; S/N, 2.5; sensitivity, 70%. All the fluctuations in scattering intensities greater than 15% were marked as excluded, and were not used for the data analysis. The DynaLS software (Protein Solutions Ltd) was used to resolve the accepted acquisitions into well-defined Gaussian distributions of hydrodynamic radii. The regularization algorithm (Protein Solutions Ltd) was also used to verify the results of the DynaLS software. The viscosities of the solutions were determined from the measured refractive indices. The total light scattering intensity (cps) was determined from cumulants analysis (Protein Solutions Ltd) as the mean of all accepted acquisitions.

Atomic force microscopy

For the AFM study, 50 μM protein at pH 2.7 was heated to 60 °C for 3 h. An aliquot of the sample (after a 100-fold dilution in pH 2.7 buffer) was applied onto a freshly cleaved mica plate. After an incubation of 1 min, the mica surface was rinsed three times with 200 μl of water, and dried under a mild stream of N_2 for 45 min before it was scanned. The AFM image was obtained on a PicoPlus AFM instrument (Molecular Imaging Inc., Arizona, USA) operating in non-contact mode.

Disaggregation of the protofibrils at pH 8

Amyloid protofibrils were first formed by heating 10 μM protein at pH 2.7 for 3 h at 60 °C. The sample was cooled to 25 °C, and then was diluted 1.25-fold into 500 mM Tris (pH 8.2) buffer containing 0.2 mM DTT. The final pH, after the dilution, was 8. After different times of incubation at pH 8, 25 °C, aliquots were withdrawn and the amount of the protofibrils present was determined by the thioflavin T fluorescence assay. After incubation for 100 h at 25 °C, the intrinsic Trp fluorescence spectrum, the far-UV CD spectrum, and the gel filtration profile were obtained. Gel filtration was done using a Superdex peptide column (Amersham Bioscience), which had an exclusion limit of 20 kDa.

Acknowledgements

This work was funded by the Tata Institute of Fundamental Research. We thank M.K. Mathew, and the members of our laboratory for discussion. We thank G. Krishnamoorthy for discussions, and M. H. Kombrabail for assistance with the AFM measurements. S.K. is a recipient of a Junior Research Fellowship funded by the Council of Scientific and Industrial Research, Government of India.

References

1. Kelly, J. W. & Balch, W. E. (2003). Amyloid as a natural product. *J. Cell Biol.* 161, 461–462.
2. Tycko, R. (2004). Progress towards a molecular-level structural understanding of amyloid fibrils. *Curr. Opin. Struct. Biol.* 14, 96–103.
3. Petkova, A. T., Leapman, R. D., Guo, Z., Yau, W., Mattson, M. P. & Tycko, R. (2005). Self-propagating, molecular-level polymorphism in Alzheimer's β-amyloid fibrils. *Science*, 307, 262–265.
4. Nelson, R., Sawaya, M. R., Balbirnie, M., Madsen, A. Ø., Riekel, C., Grothe, R. & Eisenberg, D. (2005). Structure of the cross-β spine of amyloid-like fibrils. *Nature*, 435, 773–778.
5. Sunde, M., Serpell, L. C., Bartlam, M., Fraser, P. E., Pepys, M. B. & Blake, C. C. F. (1997). Common core structure of amyloid fibrils by synchrotron X-ray diffraction. *J. Mol. Biol.* 273, 729–739.
6. Hoshino, M., Katou, H., Hagihara, Y., Hasegawa, K., Naiki, H. & Goto, Y. (2002). Mapping the core of the β_2-microglobulin amyloid fibril by H/D exchange. *Nature Struct. Biol.* 9, 332–336.
7. Kheterpal, I., Lashuel, H. A., Hartley, D. M., Walz, T., Lansbury, P. T. & Wetzel, R. (2003). Aβ protofibrils possess a stable core structure resistant to hydrogen exchange. *Biochemistry*, 42, 14092–14098.
8. Yamaguchi, K., Katou, H., Hoshino, M., Hasegawa, K., Naiki, H. & Goto, Y. (2004). Core and heterogeneity of β_2-microglobulin amyloid fibrils as revealed by H/D exchange. *J. Mol. Biol.* 338, 559–571.
9. Carulla, N., Caddy, G. L., Hall, D. R., Zurdo, J., Gairi, M., Feliz, M. *et al.* (2005). Molecular recycling within amyloid fibrils. *Nature*, 436, 554–558.
10. Lührs, T., Ritter, C., Adrian, M., Riek-Loher, D., Bohrmann, B., Döbeli, H. *et al.* (2005). 3D structure of Alzheimer's amyloid-β (1–42) fibrils. *Proc. Natl Acad. Sci. USA*, 102, 17342–17347.
11. Ritter, C., Maddelein, M., Siemer, A. B., Lührs, T., Ernst, M., Meier, B. H. *et al.* (2005). Correlation of structural elements and infectivity of the HET-s prion. *Nature*, 435, 844–848.
12. Krishnan, R. & Lindquist, S. L. (2005). Structural insights into a yeast prion illuminate nucleation and strain diversity. *Nature*, 435, 765–772.
13. Mukhopadhyay, S., Nayak, P. K., Udgaonkar, J. B. & Krishnamoorthy, G. (2006). Characterization of the formation of amyloid protofibrils from barstar by mapping residue-specific fluorescence dynamics. *J. Mol. Biol.* 358, 935–942.
14. Serpell, L. C., Blake, C. C. F. & Fraser, P. E. (2000). Molecular structure of a fibrillar Alzheimer's Aβ fragment. *Biochemistry*, 39, 13269–13275.
15. Bessen, R. A., Kocisko, D. A., Raymond, G. J., Nandan, S., Lansbury, P. T. & Caughey, B. (1995). Non-genetic propagation of strain-specific properties of scrapie prion protein. *Nature*, 375, 698–700.
16. King, C. & Diaz-Avalos, R. (2004). Protein-only transmission of three yeast prion strains. *Nature*, 428, 319–323.
17. Tanaka, M., Chien, P., Naber, N., Cooke, R. & Weissman, J. S. (2004). Conformational variations in an infectious protein determine prion strain differences. *Nature*, 428, 323–328.
18. Tanaka, M., Collins, S. R., Toyama, B. H. & Weissman, J. S. (2006). The physical basis of how prion conformations determine strain phenotypes. *Nature*, 442, 585–589.
19. Serio, T. R., Cashikar, A. G., Kowal, A. S., Sawicki, G. J., Moslehi, J. J., Serpell, L. *et al.* (2000). Nucleated conformational conversion and the replication of conformational information by a prion determinant. *Science*, 289, 1317–1321.
20. Lomakin, A., Chung, D. S., Benedek, G. B., Kirschner, D. A. & Teplow, D. B. (1996). On the nucleation and growth of amyloid β-protein fibrils: detection of nuclei and quantitation of rate constants. *Proc. Natl Acad. Sci. USA*, 93, 1125–1129.
21. Gosal, W. S., Morten, I. J., Hewitt, E. W., Smith, D. A., Thomson, N. H. & Radford, S. E. (2005). Competing pathways determine fibril morphology in the self-assembly of β_2-microglobulin into amyloid. *J. Mol. Biol.* 351, 850–864.
22. Ionescu-Zanetti, C., Khurana, R., Gillespie, J. R., Petrick, J. S., Trabachino, L. C., Minert, L. J. *et al.* (1999). Monitoring the assembly of Ig light-chain amyloid fibrils by atomic force microscopy. *Proc. Natl Acad. Sci. USA*, 96, 13175–13179.
23. Conway, K. A., Harper, J. D. & Lansbury, P. T. (2000). Fibrils formed in vitro from α-synuclein and two mutant forms linked to Parkinson's disease are typical amyloid. *Biochemistry*, 39, 2552–2563.
24. Quintas, A., Vaz, D. C., Cardoso, I., Saraiva, M. J. M. & Brito, R. M. M. (2001). Tetramer dissociation and monomer partial unfolding precedes protofibril formation in amyloidogenic transthyretin variants. *J. Biol. Chem.* 276, 27207–27213.
25. Bitan, G., Kirkitadze, M. D., Lomakin, A., Vollers, S. S., Benedek, G. B. & Teplow, D. B. (2003). Amyloid β-protein (Aβ) assembly: Aβ40 and Aβ42 oligomerize through distinct pathways. *Proc. Natl Acad. Sci. USA*, 100, 330–335.
26. Mališauskas, M., Zamotin, V., Jass, J., Noppe, W., Dobson, C. M. & Morozova-Roche, L. A. (2003). Amyloid protofilaments from the calcium-binding protein equine lysozyme: formation of ring and linear structures depends on pH and metal ion concentration. *J. Mol. Biol.* 330, 879–890.
27. Plakoutsi, G., Taddei, N., Stefani, M. & Chiti, F. (2004). Aggregation of acylphosphatase from *Sulfolobus solfataricu*: the folded and partially unfolded states can both be precursors for amyloid formation. *J. Biol. Chem.* 279, 14111–14119.
28. Bader, R., Bamford, R., Zurdo, J., Luisi, B. F. & Dobson, C. M. (2006). Probing the mechanism of amyloidogenesis through a tandem repeat of the PI3-SH3 domain suggests a generic model for protein aggregation and fibril formation. *J. Mol. Biol.* 356, 189–208.
29. Lomakin, A., Teplow, D. B., Kirschner, D. A. & Benedek, G. B. (1997). Kinetic theory of fibrillogenesis of amyloid β-protein. *Proc. Natl Acad. Sci. USA*, 94, 7942–7947.
30. Collins, S. R., Douglass, A., Vale, R. D., Weissman, J. S. (2004). Mechanism of prion propagation: amyloid growth occurs by monomer addition. *PLoS Biol.* **2**, e321, 1582–1590.
31. Baskakov, I. V., Legname, G., Baldwin, M. A., Prusiner, S. B. & Cohen, F. E. (2002). Pathway complexity of prion protein assembly into amyloid. *J. Biol. Chem.* 277, 21140–21148.
32. Fezoui, Y. & Teplow, D. B. (2002). Kinetic studies of amyloid β-protein fibril assembly: differential effects of alpha-helix stabilization. *J. Biol. Chem.* 277, 36948–36954.
33. Kaylor, J., Bodner, N., Edridge, S., Yamin, G., Hong, D. & Fink, A. L. (2005). Characterization of oligomeric

intermediates in α-synuclein fibrillation: FRET studies of Y125W/Y133F/Y136F α-synuclein. *J. Mol. Biol.* 353, 357–372.
34. Caughey, B. & Lansbury, P. T. (2003). Protofibrils, pores, fibrils, and neurodegeneration: separating the responsible protein aggregates from the innocent bystanders. *Annu. Rev. Neurosci.* 26, 267–298.
35. Kayed, R., Sokolov, Y., Edmonds, B., McIntire, T. M., Milton, S. C., Hall, J. E. & Glabe, C. G. (2004). Permeabilization of lipid bilayers is a common conformation-dependent activity of soluble amyloid oligomers in protein misfolding disease. *J. Biol. Chem.* 279, 46363–46366.
36. Quist, A., Doudevski, I., Lin, H., Azimova, R., Ng, D., Frangione, B. *et al.* (2005). Amyloid ion channels: a common structural link for protein-misfolding disease. *Proc. Natl Acad. Sci. USA*, 102, 10427–10432.
37. Chiti, F. & Dobson, C. M. (2006). Protein misfolding, functional amyloid, and human disease. *Annu. Rev. Biochem.* 75, 333–366.
38. Khurana, R. & Udgaonkar, J. B. (1994). Equilibrium unfolding studies of barstar: evidence for an alternative conformation which resembles a molten globule. *Biochemistry*, 33, 106–115.
39. Khurana, R., Hate, A. T., Nath, U. & Udgaonkar, J. B. (1995). pH dependence of the stability of barstar to chemical and thermal denaturation. *Protein Sci.* 4, 1133–1144.
40. Swaminathan, R., Periasamy, N., Udgaonkar, J. B. & Krishnamoorthy, G. (1994). Molten globule-like conformation of barstar: a study by fluorescence dynamics. *J. Phys. Chem.* 98, 9270–9278.
41. Juneja, J., Bhavesh, N. S., Udgaonkar, J. B. & Hosur, R. V. (2002). NMR identification and characterization of the flexible regions in the 160 kDa molten globule-like aggregate of barstar at low pH. *Biochemistry*, 41, 9885–9899.
42. Juneja, J. & Udgaonkar, J. B. (2003). NMR studies of protein folding. *Curr. Science*, 84, 157–172.
43. Gast, K., Modler, A. J., Damaschun, H., Kröber, R., Lutsch, G., Zirwer, D. *et al.* (2003). Effect of environmental conditions on aggregation and fibril formation of barstar. *Eur. Biophys. J.* 32, 710–723.
44. Zaidi, F. N., Nath, U. & Udgaonkar, J. B. (1997). Multiple intermediates and transition states during protein unfolding. *Nature Struct. Biol.* 4, 1016–1024.
45. Ramachandran, S., Rami, B. R. & Udgaonkar, J. B. (2000). Measurements of cysteine reactivity during protein unfolding suggest the presence of competing pathways. *J. Mol. Biol.* 297, 733–745.
46. Lakshmikanth, G. S., Sridevi, K., Krishnamoorthy, G. & Udgaonkar, J. B. (2001). Structure is lost incrementally during the unfolding of barstar. *Nature Struct. Biol.* 8, 799–804.
47. Sridevi, K. & Udgaonkar, J. B. (2002). Unfolding rates of barstar determined in native and low denaturant conditions indicate the presence of intermediates. *Biochemistry*, 41, 1568–1578.
48. Sridevi, K. & Udgaonkar, J. B. (2003). Surface expansion is independent of and occurs faster than core solvation during the unfolding of barstar. *Biochemistry*, 42, 1551–1563.
49. Wani, A. H. & Udgaonkar, J. B. (2006). HX-ESI-MS and optical studies of the unfolding of thioredoxin indicate stabilization of a partially unfolded, aggregation-competent intermediate at low pH. *Biochemistry*, 45, 11226–11238.
50. Bhuyan, A. K. & Udgaonkar, J. B. (1999). Observation of multi-state kinetics during the slow folding and unfolding of barstar. *Biochemistry*, 38, 9158–9168.
51. Hansen, S. (2004). Translational friction coefficients for cylinders of arbitrary axial ratios estimated by Monte Carlo simulation. *J. Chem. Phys.* 121, 9111–9115.
52. Georgieva, D., Schwark, D., Nikolov, P., Idakieva, K., Parvanova, K., Dierks, K. *et al.* (2005). Conformational states of the Rapana thomasiana hemocyanin and its substructures studied by dynamic light scattering and time-resolved fluorescence spectroscopy. *Biophys. J.* 88, 1276–1282.
53. Lomakin, A., Benedek, G. B. & Teplow, D. B. (1999). Monitoring protein assembly using quasielastic light scattering microscopy. *Methods Enzymol.* 309, 429–459.
54. Oosawa, F. & Kasai, M. (1962). A theory of linear and helical aggregations of macromolecules. *J. Mol. Biol.* 4, 10–21.
55. Bishop, M. F. & Ferrone, F. A. (1984). Kinetics of nucleation-controlled polymerization. A perturbation treatment for use with a secondary pathway. *Biophys. J.* 46, 631–644.
56. Flyvbjerg, H., Jobs, E. & Leibler, S. (1996). Kinetics of self-assembling microtubules: an "inverse problem" in biochemistry. *Proc. Natl Acad. Sci. USA*, 93, 5975–5979.
57. Ferrone, F. (1999). Analysis of protein aggregation kinetics. *Methods Enzymol.* 309, 256–274.
58. Durbin, S. D. & Feher, G. (1996). Protein crystallization. *Annu. Rev. Phys. Chem.* 47, 171–204.
59. Chen, S., Ferrone, F. A. & Wetzel, R. (2002). Huntington's disease age-of-onset linked to polyglutamine aggregation nucleation. *Proc. Natl. Acad. Sci. USA*, 99, 11884–11889.
60. Hemker, D. J. & Frank, C. W. (1990). Dynamic light scattering studies of the fractal aggregation of poly (methacrylic acid) and poly (ethylene glycol). *Macromolecules*, 23, 4404–4410.
61. Speed, M. A., Wang, D. I. & King, J. (1995). Multimeric intermediates in the pathway to the aggregated inclusion body state for P22 tailspike polypeptide chains. *Protein Sci.* 4, 900–908.
62. Xu, S., Bevis, B. & Arnsdorf, M. F. (2001). The assembly of amyloidogenic yeast Sup35 as assessed by scanning (atomic) force microscopy: an analogy to linear colloidal aggregation? *Biophys. J.* 81, 446–454.
63. Nichols, M. R., Moss, M. A., Reed, D. K., Lin, W., Mukhopadhyay, R., Hoh, J. H. & Rosenberry, T. L. (2002). Growth of β-amyloid (1-40) protofibrils by monomer elongation and lateral association. Characterization of distinct products by light scattering and atomic force microscopy. *Biochemistry*, 41, 6115–6127.
64. Carrotta, R., Manno, M., Bulone, D., Martorana, V. & Biagio, P. L. S. (2005). Protofibril formation of amyloid β-protein at low pH via a non-cooperative elongation mechanism. *J. Biol. Chem.* 280, 30001–30008.
65. Modler, A. J., Gast, K., Lutsch, G. & Damaschun, G. (2003). Assembly of amyloid protofibrils via critical oligomers - a novel pathway of amyloid formation. *J. Mol. Biol.* 325, 135–148.
66. Hurshman, A. R., White, J. T., Powers, E. T. & Kelly, J. W. (2004). Transthyretin aggregation under partially denaturing conditions is a downhill polymerization. *Biochemistry*, 43, 7365–7381.
67. Howard, J. (2001). Polymerization of cytoskeletal filaments. In *Mechanics of Motor Proteins and the Cytokeleton*. pp. 155, Sinauer Associates, Massachusetts.
68. Teplow, D. B., Lazo, N. D., Bitan, G., Bernstein, S., Wyttenbach, T., Bowers, M. T. *et al.* (2006). Elucidating

amyloid β-protein folding and assembly: a multidisciplinary approach. *Acc. Chem. Res.* 39, 635–645.
69. Kusumoto, Y., Lomakin, A., Teplow, D. B. & Benedek, G. B. (1998). Temperature dependence of amyloid β-protein fibrillization. *Proc. Natl. Acad. Sci. USA*, 95, 12277–12282.
70. Kayed, R., Head, E., Thompson, J. L., McIntire, T. M., Milton, S. C., Cotman, C. W. & Glabe, C. G. (2003). Common structure of soluble amyloid oligomers implies a common mechanism of pathogenesis. *Science*, 300, 486–489.
71. O'Nuallain, B. & Wetzel, R. (2002). Conformational Abs recognizing a generic amyloid fibril epitope. *Proc. Natl Acad. Sci. USA*, 99, 1485–1490.

Edited by J. Weissman

(Received 30 October 2006; received in revised form 12 January 2007; accepted 16 January 2007)
Available online 20 January 2007